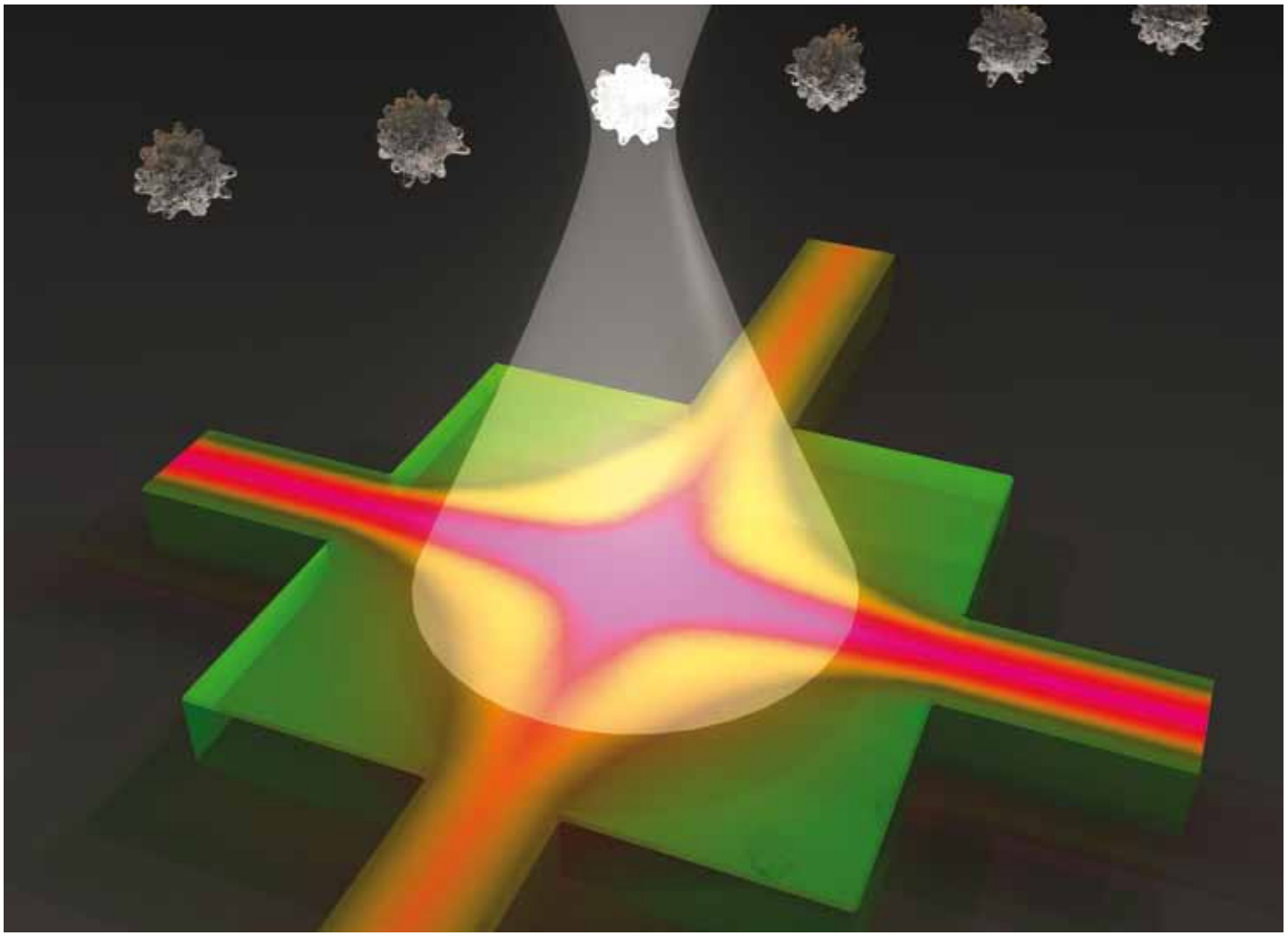

Featuring research from the group of Professor Tony Jun Huang at The Pennsylvania State University.

Title: Tunable two-dimensional liquid gradient refractive index (L-GRIN) lens for variable light focusing

A tunable two-dimensional (2D) liquid gradient refractive index (L-GRIN) lens was developed *via* microfluidic manipulation of a 2D refractive index gradient. This lens provides variable light focusing for potential applications such as on-chip flow cytometry and optical tweezers.

As featured in:

See Huang *et al.*, *Lab Chip*, 2010, **10**, 2387–2393

Tunable two-dimensional liquid gradient refractive index (L-GRIN) lens for variable light focusing†‡

Hua Huang,[ab] Xiaole Mao,[bc] Sz-Chin Steven Lin,[b] Brian Kiraly,[b] Yiping Huang[a] and Tony Jun Huang*[bc]

Received 13th April 2010, Accepted 6th July 2010
DOI: 10.1039/c005071g

We report a two-dimensional (2D) tunable liquid gradient refractive index (L-GRIN) lens for variable focusing of light in the out-of-plane direction. This lens focuses a light beam through a liquid medium with a 2D hyperbolic secant (HS) refractive index gradient. The refractive index gradient is established in a microfluidic chamber through the diffusion between two fluids with different refractive indices, *i.e.* $CaCl_2$ solution and deionized (DI) water. The 2D HS refractive index profile and subsequently the focal length of the L-GRIN lens can be tuned by changing the ratio of the flow rates of the $CaCl_2$ solution and DI water. The focusing effect is experimentally characterized through side-view and top-view image analysis, and the experimental data match well with the results from ray-tracing optical simulations. Advantages of the 2D L-GRIN lens include simple device fabrication procedure, low fluid consumption rate, convenient lens-tuning mechanism, and compatibility with existing microfluidic devices. We expect that with further optimizations, this 2D L-GRIN lens can be used in many optics-based lab-on-a-chip applications.

Introduction

Tunable microlenses have drawn much attention in recent years due to their applications in optics-based lab-on-a-chip systems. Tunable microlenses are capable of focusing incident light, shifting the focal point, and collecting weak light at the micrometre scale. They can be further combined with other on-chip components to perform functions such as biological detection,[1,2] particle manipulation,[3,4] and microscopic bioimaging.[5–7] Thus far, many methods have been utilized to construct tunable microlenses. Elastomeric materials, such as polydimethylsiloxane (PDMS), have been used to form pressure-actuated tunable lens surfaces.[8–10] In recent years, liquids have become a popular active material in tunable microlenses due to their advantages of reconfigurability and optically smooth meniscus surfaces. For example, the electrowetting phenomenon[11–13] has proven to be a promising mechanism for changing the liquid contact angle, and hence the radius of curvature of the liquid meniscus along with the focal length of the meniscus microlens.[14,15]

Most recently, the concept of reconfigurable liquid–liquid optofluidic[16–21] devices, such as liquid-core/liquid-cladding waveguides and light sources, has been developed.[22,23] In these liquid–liquid optofluidic devices, light can be manipulated purely by liquid flow, thus eliminating the need for mechanical or electrical light-manipulation mechanisms. This characteristic makes liquid–liquid optofluidic devices naturally compatible with other flow-based lab-on-a-chip components. In this regard, various tunable optofluidic microlenses based on liquid–liquid interfaces have been successfully demonstrated.[24] The key to these liquid–liquid microlenses is to create a hydrodynamically tunable, curved liquid–liquid interface between two side-by-side flowing fluids having different refractive indices. The tunable liquid–liquid interface can then act as a refractive lens to variably focus light. Previously, we demonstrated a tunable optofluidic cylindrical microlens[24] by using the Dean flow effect[25–28] induced in a curved microchannel to bend a $CaCl_2/H_2O$ liquid–liquid interface. Reconfigurable liquid–liquid lenses which exploited the convex shape of liquid–liquid interfaces in a microfluidic expansion chamber have also been demonstrated by the Whitesides group and others.[29,30]

The major advantage of these liquid–liquid interface-based microlenses is that the lenses can be tuned with simple adjustment of the flow conditions. On the other hand, however, these liquid–liquid interface-based microlenses present two challenges. First, diffusion of solute across the fluid–fluid interface tends to smear the fluid–fluid interface boundary. This forces the lens design to use a high flow rate to minimize the diffusion time and maintain a relatively distinct liquid–liquid interface. Second, most of the current liquid–liquid interface-based microlenses are only capable of line focusing (1D focusing), instead of point focusing (2D focusing). This is because current microfluidic technology has not yet been able to provide a means to conveniently create the precisely controlled, 3D liquid–liquid interface needed for 2D focusing.

To address the first challenge of the liquid–liquid interface-based microlenses, we recently introduced a concept called liquid gradient refractive index (L-GRIN) lens.[31] Instead of attempting to eliminate diffusion in the microfluidic channel, the L-GRIN

[a]*ASIC and System State Key Lab, Department of Microelectronics, Fudan University, Shanghai, 200433, P.R. China*
[b]*Department of Engineering Science and Mechanics, The Pennsylvania State University, University Park, PA, 16802, USA. E-mail: junhuang@psu.edu; Fax: +1 814 865 9974; Tel: +1 814 863 4209*
[c]*Department of Bioengineering, The Pennsylvania State University, University Park, PA, 16802, USA*

† Published as part of a special issue dedicated to Emerging Investigators: Guest Editors: Aaron Wheeler and Amy Herr.

‡ Electronic supplementary information (ESI) available: Details of device fabrication and additional information for optical ray-tracing simulation. See DOI: 10.1039/c005071g

lens works by taking advantage of the diffusion at the microscale to form a refractive index gradient in the liquid medium. In the L-GRIN lens, a high-refractive-index solution was injected side-by-side with low-refractive-index solutions. The diffusion of solute between the co-injected flows can form a refractive index gradient, which can focus light in a way similar to the traditional gradient refractive index (GRIN) lenses made of solid materials such as glass or polymers.[32,33] In a microfluidic environment, the diffusion profile can be conveniently controlled *via* the manipulation of the fluid flows. Therefore, the diffusion profile of the solute, and hence the refractive index profile within the L-GRIN lens, can be easily adjusted by changing flow parameters. In our previous study, the L-GRIN lens concept was proven to be a useful method for variable light focusing.[31] In contrast to the conventional liquid–liquid interface-based microlenses, the L-GRIN lens operates through the diffusion in multiple flows, rather than relying on a clearly defined, curved fluid–fluid interface. Therefore the flow consumption rate is much lower in the L-GRIN lens than in the previously described liquid–liquid interface-based microlenses. In our previous work, we successfully used a converging microfluidic channel to implement an L-GRIN lens which focuses light along the device plane in one dimension (line focusing).

In this work, we aim to further develop the concept of the L-GRIN lens to create a tunable 2D L-GRIN lens that addresses the second challenge faced by the liquid–liquid interface-based microlenses: 2D light focusing (point focusing). One of the significant advantages of the L-GRIN lens approach over the traditional refractive lens is that it relies on the spatial distribution of the refractive index, rather than the geometry of the lens surface to focus light. This gives us an opportunity to use a tunable, 2D refractive index gradient to achieve the 2D light focusing (which can be conveniently created with a simple planar microfluidic structure), rather than a complicated 3D liquid–liquid interface.

Materials and methods

The key to constructing an L-GRIN lens is to form a light-focusing hyperbolic secant (HS) refractive index profile. In this work, the diffusion of $CaCl_2$ between a high refractive index solution ($CaCl_2$) and a low refractive index liquid (DI water) is used to achieve the 2D focusing. Different from the one-dimensional, line-focusing L-GRIN lens introduced in our previous work[31] that focuses light along the device plane, the current device can focus light two-dimensionally (point-focusing) in the direction that is perpendicular to the device plane (X–Y plane). An axis-symmetric 2D HS refractive index profile was achieved using a microfluidic structure shown in Fig. 1(a). Six inlets and two outlets were connected to an L-GRIN lens chamber to allow the introduction of fluids with high and low refractive indices. The two outlets allow the fluids to symmetrically exit the chamber. In our experiments, a 5 M $CaCl_2$ solution ($n_D \approx 1.445$) was used as the high-refractive-index fluid, and DI water ($n_D \approx 1.335$)[22] was used as the low-refractive-index fluid. The $CaCl_2$ solutions were injected into the lens chamber through two center inlets and converged with the low-refractive-index fluids (H_2O) from side inlets. This allows $CaCl_2$ to diffuse from the $CaCl_2$ solution to DI water to form an axis-symmetric HS distribution

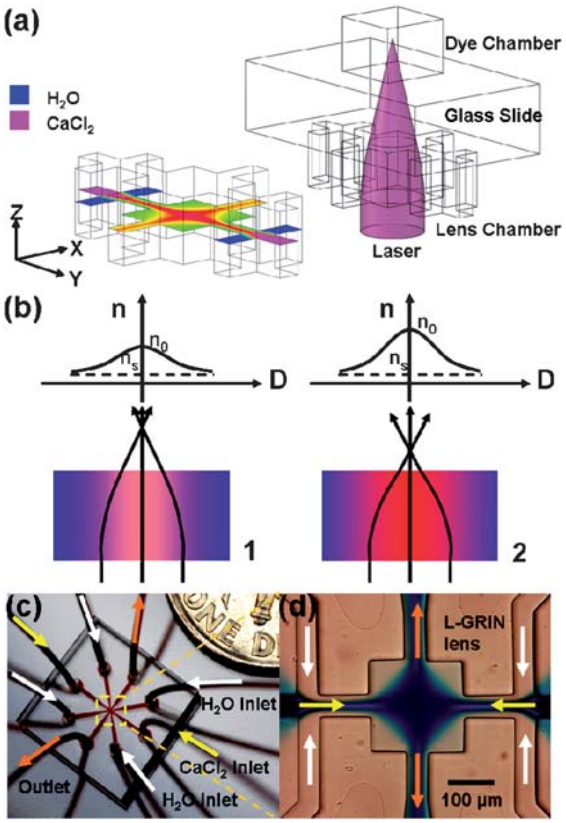

Fig. 1 Principle of the 2D L-GRIN lens. (a) The 2D L-GRIN lens structure is composed of an L-GRIN lens chamber, two inlets for $CaCl_2$ solution, four inlets for DI water, and two outlets. The diffusion of $CaCl_2$ inside the L-GRIN lens chamber results in a 2D axis-symmetric hyperbolic secant (HS) refractive index profile in the X–Y plane, which can be used to focus the light beam along the Z direction. The lens is bonded to a glass substrate and a dye chamber is bonded on the opposite side of the glass substrate for visualization purpose. The input light is generated *via* a laser diode aligned vertically to the device plane. (b) The side view of the refractive index distribution in the L-GRIN lens chamber. The focal point of the 2D L-GRIN lens can be shifted along Z-axis (*e.g.*, from b1 to b2 by adjusting the refractive index gradient within the liquid medium). (c) The fluid injection setup of the 2D L-GRIN lens (dye chamber is not included in this image). (d) A microscopic image of the 2D diffusion pattern in the lens chamber.

of $CaCl_2$. Therefore, in the X–Y plane of the lens chamber, the highest refractive index is achieved in the center, and the refractive index decreases radially away from the center. This axial-symmetric HS refractive index profile is formed in the lens chamber and acts as an optical lens to focus light two-dimensionally as shown in Fig. 1(b).

The HS refractive index distribution in the X–Y plane of the lens chamber determines the optical properties[34] of the 2D L-GRIN lens, and is described by the following equation,[35]

$$n^2(d) = n_s^2 + (n_o^2 - n_s^2)\,\mathrm{sech}^2(\alpha d),$$

in which $n(d)$ is the refractive index of the solution with a transverse distance d from the center axis of the lens chamber, n_0 is the highest refractive index at the center axis of the 2D L-GRIN lens, n_s is the background (lowest) refractive index of the solution, and α is the gradient parameter determined by the refractive index

profile. With such a 2D refractive index profile in the X–Y device plane, the vertical light beam can be focused two-dimensionally along the z-axis. The position of the focal point can be tuned along the z-direction by changing the HS refractive index profile (Fig. 1(b)), which can be achieved by adjusting the flow rate ratios between the high-refractive-index ($CaCl_2$) and the low-refractive-index fluids (H_2O).

The experimental setup is shown in a 3D schematic in Fig. 1(a). The incident light from a 532 nm laser diode was aligned to the central axis of the 2D L-GRIN lens structure and shined normally (z direction) on the lens chamber. In order to observe the focusing effect of the 2D L-GRIN lens, the device had three layers, including (from bottom to top) the 2D L-GRIN lens chamber (thickness = 155 μm, width and length = 200 μm), the glass substrate layer (thickness = 220 μm), and the dye chamber (thickness = 155 μm, width and length = 200 μm). The dye chamber was filled with a fluorescent dye solution (Rhodamine B, 10 μg ml^{-1}) so that the trajectories of the focused light beams could be observed during the focusing process. The 2D L-GRIN lens chamber and the dye chamber were made using standard soft lithography and mold replica procedures[36] (please see ESI† for detailed fabrication procedure). The fluids were injected into the L-GRIN lens chamber using precision syringe pumps (KD Scientific 210). The experiments were conducted on an inverted optical microscope (Nikon TE 2000U), with the images taken by a color digital camera (Nikon D50) mounted on the microscope. Fig. 1(c) illustrates the fluid injection setup of the 2D L-GRIN lens (dye chamber is not included in this image), and Fig. 1(d) shows a microscopic image of the 2D diffusion pattern in the lens chamber (food dye was added into the $CaCl_2$ solution to highlight the diffusion pattern).

To evaluate the performance of this 2D L-GRIN lens and optimize the experimental parameters, two types of numerical simulations were conducted. First, computational fluid dynamics (CFD) simulations were done with a commercial software package (ESI-CFD) and were used for calculating the $CaCl_2$ concentration distribution, which is linearly proportional to the refractive index distribution in the L-GRIN lens. Based on the data obtained from the CFD simulation, an optical ray-tracing simulation was performed to simulate the trajectories of the light beams during the focusing process. The ray-tracing algorithm for an HS refractive index gradient was based on the ABCD law and was implemented with a MATLAB program. The analysis of the experimental result was conducted using an image analysis package ImageJ.[37]

Results and discussions

In order to form the axis-symmetric refractive index profile in the lens chamber, the $CaCl_2$ solution was co-injected with the DI water into the lens chamber from two opposite directions as shown in Fig. 2(a). The DI water streams compress the $CaCl_2$ solution from both sides, and $CaCl_2$ molecules diffuse across the interface of the two fluids. Fig. 2(a) shows the simulated concentration distribution of $CaCl_2$ during the flow injection process. The simulation result indicates that upon contacting the DI water, $CaCl_2$ starts to diffuse from the $CaCl_2$ solution into DI water. After two opposite $CaCl_2$ solution/DI water co-flows enter the lens chamber, they are forced to change their flow directions and exit the chamber from two symmetric outlets. The diffusion of $CaCl_2$ in this process results in the formation of a light-focusing, 2D refractive index gradient in the lens chamber.

To evaluate the focusing capability of this 2D refractive index gradient, the refractive index distribution (Fig. 2(b)) within the lens chamber was plotted using the $CaCl_2$ concentration distribution obtained from the CFD result in Fig. 2(a). Fig. 2(b) indicates that the refractive index in the lens chamber shows an axis-symmetric pattern, in which refractive index is higher in the center and lower towards the outer edges. We further plot the line profiles (Fig. 2(c)) of the refractive index within the lens chamber, with β increasing from 0° to 90° with a 5° increment (β is defined in Fig. 2(b)). It is found that, except for the lines near the directions of the inlets and outlets ($\beta = 0°$ and 90°), most of the refractive index profiles follow an HS distribution and match well with each other. This characteristic ensures that nearly all of the incoming light is focused to a single focal point. In order to investigate the influence of fluid injection parameters on the refractive index profile, and hence the position of the focal point, the refractive index profiles of $CaCl_2$ at different fluid injection conditions were simulated. Fig. 2(d) shows the change of diagonal concentration distribution ($\beta = 45°$) of $CaCl_2$ in the fluid chamber with decreasing DI water/$CaCl_2$ flow rate ratio (from bottom to top, DI water flow rate = 8.0, 6.4, 4.8, 3.2, 2.4, 1.6, and 0.8 μl min^{-1}, respectively; $CaCl_2$ solution flow rate = 8.0 μl min^{-1} for all cases).

Fig. 2(d) suggests that the HS refractive index distribution within the lens chamber can be conveniently adjusted by varying the fluid rates. Further analysis in Fig. 2(e) shows the relation between the change of refractive index contrast (difference between the maximum and minimum of the refractive index profile) and the change of the fluid rate ratio (DI water/$CaCl_2$ solution). Since a change of the refractive index contrast corresponds to a linear change in the focal length, Fig. 2(e) suggests that the focal length does not linearly increase with the flow rate ratio—it is most responsive when the flow rate ratio is low (0.1–0.5) and becomes less responsive when the flow rate ratio is close to 1.0. This observation is useful in determining the operation parameters of the 2D L-GRIN lens.

Fig. 3(a–c) are the CFD simulated refractive index distributions inside the lens chamber at different flow conditions (DI water flow rate = 8.0 μl min^{-1}, 3.2 μl min^{-1}, and 2.4 μl min^{-1}, respectively, and $CaCl_2$ solution flow rate = 8.0 μl min^{-1} in all three cases). These simulated 2D refractive index distributions can be fitted well with a 2D HS profile (please see the ESI† for details), and the 2D-fitted HS profiles were used for the ray-tracing simulation to evaluate the performance of the 2D L-GRIN lens for light focusing. The ray-tracing simulations show the trajectories of light beams in the three-layer structure previously introduced (the L-GRIN lens chamber, the glass substrate, and the dye chamber, respectively). The ray-tracing simulations were conducted using the corresponding flow rate parameters from Fig. 3(a–c), and the simulated light-focusing patterns (in X–Z cross-sectional plane) are shown in Fig. 3(d–f). The results show that inside the liquid medium within the L-GRIN lens chamber, collimated light beams from the laser source bend gradually towards the central optical axis. After exiting the 2D L-GRIN lens, the light propagates through the

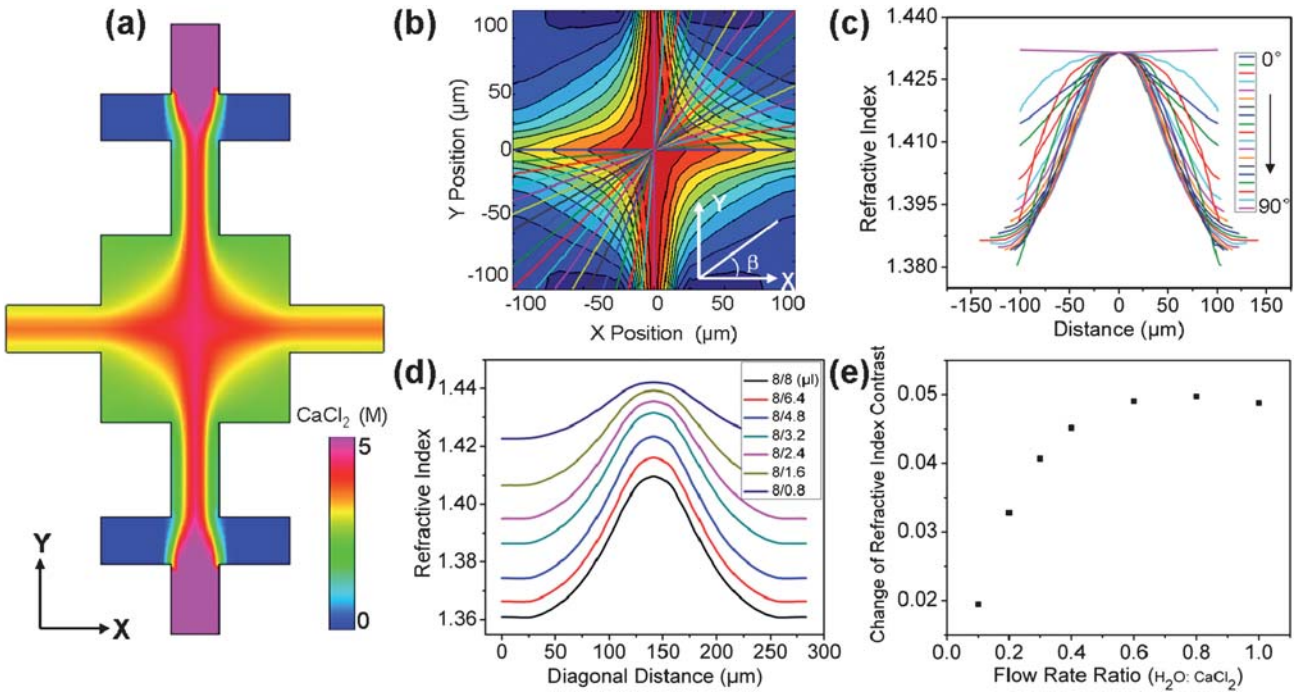

Fig. 2 (a) The simulated $CaCl_2$ concentration distribution in the fluid chamber ($CaCl_2$ flow rate = 8 μl min^{-1} and DI water flow rate = 3.2 μl min^{-1}). (b) The refractive index distribution in the lens chamber derived from the CFD simulation. (c) The line profile of refractive index in the X–Y plane along different directions (from 0° to 90° with a 5° increment). (d) Change of the refractive index profile with different fluid rates ($\beta = 45°$). (e) The change of the refractive index contrast is not linear with respect to the change of the flow rate ratio between water and $CaCl_2$ solution.

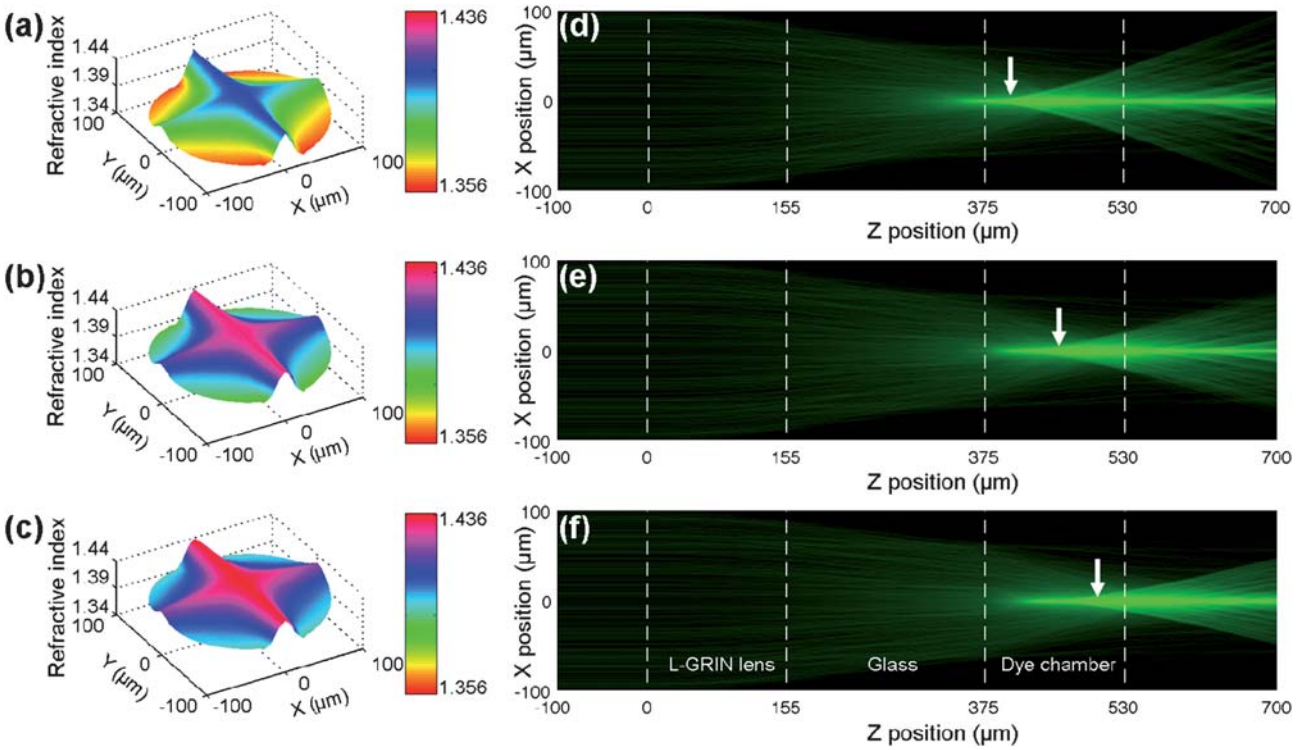

Fig. 3 Ray-tracing simulation of the variable light focusing process. (a–c) The CFD simulated 2D HS refractive index profile within the lens chamber for different flow conditions (DI water flow rate = 8.0 μl min^{-1}, 3.2 μl min^{-1}, and 2.4 μl min^{-1}, respectively, and $CaCl_2$ solution flow rate = 8.0 μl min^{-1} in all three cases). (d–f) The simulated trajectories of the light beam during the focusing process with three different fluid flow conditions shown in (a–c), respectively. The structure in the simulation is composed of three parts: the L-GRIN lens, the glass substrate, and the dye chamber.

glass substrate and converges within the dye chamber at the focal point. Changing the fluid injection ratios results in a change in refractive index gradient (Fig. 3(a–c)), causing the light to converge differently and resulting in a shift of the focal point inside the dye chamber along the z-direction (Fig. 3(d–f)). These simulated results suggest that the focal length increases when the flow rate of DI water decreases. The simulations also predict the tuning range of the focal point along the z-axis to be ~130 μm.

In order to characterize the performance of the L-GRIN lens, a series of experiments were conducted with the experimental setup for side-view ray-tracing illustrated in Fig. 4(a). The device used for experimental characterization, as previously described, consists of three components: the L-GRIN lens, the glass substrate, and the dye chamber. The collimated light beam from a semiconductor laser diode (532 nm) was shined on the X–Y plane of the L-GRIN lens chamber along the z-direction. After exiting the L-GRIN lens chamber, the light enters the dye chamber through the glass layer, where its trajectory can be visualized by the fluorescent emission of Rhodamine dyes (excitation wavelength of 532 nm and emission wavelength of 560 nm). It should be noted that the performance of the L-GRIN lens can be affected by temperature. Temperature has an influence on the refractive index gradient profile of the L-GRIN lens because both the diffusion coefficient of the solute ($CaCl_2$) and the refractive index of the liquid medium vary with temperature.[38,39] Therefore, changes in temperature can result in a variation of the lens performance, such as a variation in the lens' focal length.

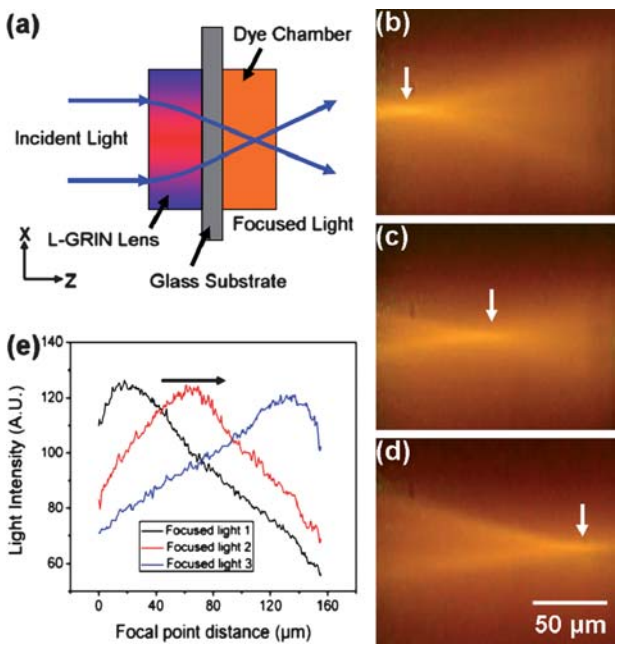

Fig. 4 Experimental characterization of the variable light focusing process. (a) The device includes three layers (*i.e.* the L-GRIN lens chamber, the glass substrate, and the dye chamber for visualization of the focused light beams). (b–d) Change of the light-focusing patterns and shifting of the focal point positions with different flow rate conditions (DI water flow rate = 8.0 μl min^{-1}, 3.2 μl min^{-1}, and 2.4 μl min^{-1}, respectively, and $CaCl_2$ solution flow rate = 8.0 μl min^{-1} in all three cases) are visualized in the dye chamber. (e) Light intensity plots along the z-axis, corresponding to the images in (b–d), indicate the shift of the focal point during the experiments.

Throughout our experiments, the fluid temperatures remained constant (~25 °C) and therefore the experimental results of the L-GRIN lens were highly repeatable. In the future studies, we will use CFD and ray-tracing simulations to investigate the influence of changes in the solute diffusion coefficient and refractive index of the liquid medium, caused by the temperature variation, on the performance of the L-GRIN lens.

The side-view ray-tracing experiments were conducted with the same parameters that were used in the CFD and ray-tracing simulations in Fig. 3 (DI water flow rate = 8.0 μl min^{-1}, 3.2 μl min^{-1}, and 2.4 μl min^{-1}, respectively; $CaCl_2$ solution flow rate = 8.0 μl min^{-1}). Fig. 4(b–d) illustrate the trajectories of the light beams within the dye chamber. The results show that the light beam can be well focused to a point whose position can be shifted along the z-axis with different flow rates. Fig. 4(e) shows the light intensity plots along the z-axis, and the maximum intensity indicates the position of focal point. The results show that the focal point can be shifted approximately 120 μm, which matches well with the simulated result in Fig. 3 (~130 μm). For this 2D L-GRIN lens, the establishment of the refractive index gradient for light focusing relies solely on the diffusion of the solute ($CaCl_2$) between high and low refractive-index solutions; this process is affected by multiple factors such as diffusion coefficient, fluid viscosity, and compliance of the fluid injection tubings. Experimentally, we have observed that the transition between different operation states (different focal lengths) can be achieved within 2–3 seconds. This observation is in agreement with our previous work on L-GRIN lens with 1D focusing ability.[31] Additionally, once the fluid injection rates of the device are set and the refractive index profile is stabilized, the lens can remain stable for a long period of time (several hours or more).

From the experimental results, the maximum numerical aperture (NA = $n\sin\theta$, where n, the refractive index in the dye chamber, is approximately 1.33, and θ is half of the focused beam exit angle) is measured to be 0.249 in Fig. 4(b). The NA of a lens is one of the most important parameters in evaluating its focusing ability, and a high NA is often required for optical trapping[40,41] and high-resolution imaging. Further improvement of the NA can be achieved by increasing the depth of the L-GRIN lens chamber (currently 155 μm) or the refractive index contrast between the two fluids; both alterations would lead to more dramatic bending of the light beams.

We observe through both simulations and experiments that the L-GRIN lens shows some aberration (light beams not perfectly focused to a single focal point). We believe this is due to the fact that the profiles of the refractive indices achieved with current L-GRIN lens fluidic channel design are slightly different from the theoretical hyperbolic secant profiles. In order to minimize the aberration and to improve the performance of the L-GRIN lens, further geometric optimization of the L-GRIN lens' fluidic channel is needed to achieve ideal refractive index profiles to perfectly focus all the light beams to a single focal point.

In order to further characterize the focusing performance of the 2D L-GRIN lens, we characterized the top-view images of the focused light spots in the dye chamber (X–Y plane) at different flow conditions. Fig. 5(a) shows the unfocused light distribution in the dye chamber when the 2D L-GRIN lens is not operational (stagnant flow in the lens chamber). Fig. 5(b–d) show the transition of the light-focusing pattern from under-focused to

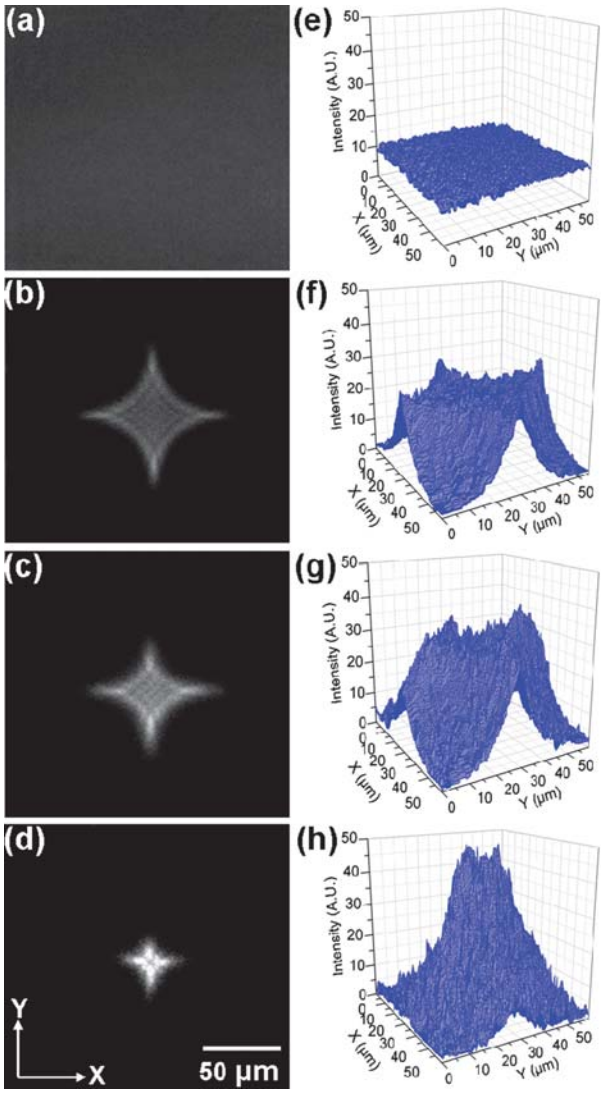

Fig. 5 Top-view images of the light spots in the dye chamber after the light passing through the 2D L-GRIN lens at different flow conditions. (a) Unfocused (stagnant flow); (b–d) from under-focused to well-focused light. DI water flow rate = 6.4 μl min^{-1}, 4.8 μl min^{-1}, and 3.2 μl min^{-1}, respectively; and $CaCl_2$ solution flow rate = 8.0 μl min^{-1}. (e–h) The 2D light intensity distribution corresponding to (a–d), respectively.

well-focused at different flow injection conditions (DI water flow rates = 6.4 μl min^{-1}, 4.8 μl min^{-1}, and 3.2 μl min^{-1}, respectively; $CaCl_2$ solution flow rates = 8.0 μl min^{-1}). These images provide direct proof of the tunable 2D light focusing. From these images it is observed that the shape of the light spot is similar to the refractive index distribution in the lens chamber. The minimum spot size (Fig. 5(d)) achieved with this 2D L-GRIN lens is ~20 μm, which is suitable for applications such as on-chip flow cytometry.[24,42] Fig. 5(e–h) show the changes of the 2D intensity distribution of the light beam at different focusing conditions. The light intensity is increased by a factor of 4.5 from the non-focused condition (Fig. 5(e)) to the well-focused one (Fig. 5(h)). It is noted that the shape of the focused light beam obtained with this 2D L-GRIN lens is similar to a square with stronger intensity distribution along the two diagonal directions, which is different from the circular light spots obtained with most existing 2D lenses. Further improvement of the 2D refractive index distribution is needed to achieve a more desirable light-focusing pattern. This can be achieved by optimizing the geometry of the L-GRIN lens chamber.

In this article, we have demonstrated that three different lens states (focal lengths and numerical apertures) can be achieved with three different sets of fluid injection parameters. These one-to-one lens state/fluid injection parameter correlations can serve as a preliminary look-up table for lens operation. A more comprehensive and detailed look-up table can be established by further correlating different lens states (focal lengths and numerical apertures) with different flow injection rates through simulation and experimental measurement. We have experimentally demonstrated that our L-GRIN lens is highly repeatable, and one should always expect the same lens state (same focal length and numerical aperture) with a specific set of fluid injection parameters, regardless of the initial state of the lens. Additionally, the lens is very stable over time. Therefore, we believe that our L-GRIN lens is capable of delivering reliable, repeatable performance.

Conclusions

In this article, we introduced a tunable 2D L-GRIN microlens which can be used to two-dimensionally focus light normally incident on the device plane. By utilizing the diffusion phenomena in fluids, this L-GRIN lens can achieve 2D light focusing with a simple, planar microfluidic chamber, rather than involving complex three-dimensional microstructures used in previously reported 2D microlenses. The 2D L-GRIN lens can be conveniently fabricated using standard soft-lithography and can be readily integrated with other microfluidic devices. The 2D L-GRIN lens also has other advantages such as low flow consumption and a simple lens control mechanism. Simply by adjusting the fluid injection ratio, the focal point of this lens can be varied along the out-of-plane direction (z-direction). These advantages make the 2D L-GRIN lens suitable for a wide variety of on-chip applications such as on-chip detection, and potentially the manipulation of particles/molecules.[43–50] The 2D L-GRIN lens, as with the 1D L-GRIN lens introduced in our previous work,[31] represents a novel concept by utilizing the precise manipulation of refractive index distribution in microfluidic environments for on-chip light manipulation. We envision that with further developments, this concept can facilitate a new class of optofluidic devices for on-chip optical applications.

Acknowledgements

This research was supported by US Department of Agriculture (USDA/NRI), National Science Foundation, Air Force Office of Scientific Research (AFOSR), and the Penn State Center for Nanoscale Science (MRSEC). Components of this work were conducted at the PennState node of the NSF-funded National Nanotechnology Infrastructure Network.

References

1 A. Llobera, V. J. Cadarso, M. Darder, C. Domínguez and C. F. Sánchez, *Lab Chip*, 2008, **8**, 1185–1190.
2 S. Mandal and D. Erickson, *Opt. Express*, 2008, **16**, 1623–1631.

3 F. Arai, C. Ng, H. Maruyama, A. Ichikawa, H. El-Shimy and T. Fukuda, *Lab Chip*, 2005, **5**, 1399–1403.
4 B. S. Schmidt, A. H. J. Yang, D. Erickson and M. Lipson, *Opt. Express*, 2007, **15**, 14322–14334.
5 X. Heng, D. Erickson, L. R. Baugh, Z. Yaqoob, P. W. Sternberg, D. Psaltis and C. Yang, *Lab Chip*, 2006, **6**, 1274–1276.
6 S. Pang, X. Cui, J. DeModena, Y. M. Wang, P. Sternberg and C. Yang, *Lab Chip*, 2010, **10**, 411–414.
7 J. Wu, X. Cui, L. M. Lee and C. Yang, *Opt. Express*, 2008, **16**, 15595–15602.
8 G. Beadie, M. L. Sandrock, M. J. Wiggins, R. S. Lepkowicz, J. S. Shirk, M. Ponting, Y. Yang, T. Kazmierczak, A. Hiltner and E. Baer, *Opt. Express*, 2008, **16**, 11847–11857.
9 K. H. Jeong, G. Liu, N. Chronis and L. P. Lee, *Opt. Express*, 2004, **12**, 2494–2500.
10 N. Chronis, G. L. Liu, K. Jeong and L. P. Lee, *Opt. Express*, 2003, **11**, 2370–2378.
11 M. G. Pollack, R. B. Fair and A. D. Shenderov, *Appl. Phys. Lett.*, 2000, **77**, 1725–1726.
12 S. K. Fan, H. Yang, T. T. Wang and W. Hsu, *Lab Chip*, 2007, **7**, 1330–1335.
13 R. A. Hayes and B. J. Feenstra, *Nature*, 2003, **425**, 383–385.
14 F. Krogmann, R. Shaik, L. Lasinger, W. Mönch and H. Zappe, *Sens. Actuators, A*, 2008, **143**, 129–135.
15 S. Kuiper and B. H. W. Hendriks, *Appl. Phys. Lett.*, 2004, **85**, 1128–1130.
16 H. Schmidt and A. R. Hawkins, *Microfluid. Nanofluid.*, 2008, **4**, 3–16.
17 A. R. Hawkins and H. Schmidt, *Microfluid. Nanofluid.*, 2008, **4**, 17–32.
18 D. Psaltis, S. R. Quake and C. Yang, *Nature*, 2006, **442**, 381–386.
19 C. Monat, P. Domachuk and B. J. Eggleton, *Nat. Photonics*, 2007, **1**, 106–114.
20 J. Shi, Z. Stratton, S. C. S. Lin, H. Huang and T. J. Huang, *Microfluid. Nanofluid.*, 2010, **9**, 313–318.
21 M. I. Lapsley, S. C. S. Lin, X. Mao and T. J. Huang, *Appl. Phys. Lett.*, 2009, **95**, 083507.
22 D. B. Wolfe, R. S. Conroy, P. Garstecki, B. T. Mayers, M. A. Fischbach, K. E. Paul, M. Prentiss and G. M. Whitesides, *Proc. Natl. Acad. Sci. U. S. A.*, 2004, **101**, 12434–12438.
23 D. V. Vezenov, B. T. Mayers, D. B. Wolfe and G. M. Whitesides, *Appl. Phys. Lett.*, 2005, **86**, 041104.
24 X. Mao, J. R. Waldeisen and T. J. Huang, *Lab Chip*, 2007, **7**, 1260–1262.
25 P. B. Howell, Jr, D. R. Mott, J. P. Golden and F. S. Ligler, *Lab Chip*, 2004, **4**, 663–669.
26 D. Di Carlo, D. Irimia, R. G. Tompkins and M. Toner, *Proc. Natl. Acad. Sci. U. S. A.*, 2007, **104**, 18892–18897.
27 A. P. Sudarsan and V. M. Ugaz, *Proc. Natl. Acad. Sci. U. S. A.*, 2006, **103**, 7228–7233.
28 Y. Yamaguchi, F. Takagi, K. Yamashita, H. Nakamura, H. Maeda, K. Sotowa, K. Kusakabe, Y. Yamasaki and S. Morooka, *AIChE J.*, 2004, **50**, 1530–1535.
29 S. K. Y. Tang, C. A. Stan and G. M. Whitesides, *Lab Chip*, 2008, **8**, 395–401.
30 C. Song, N. T. Nguyen, S. H. Tan and A. K. Asundi, *Lab Chip*, 2009, **9**, 1178–1184.
31 X. Mao, S. C. S. Lin, M. I. Lapsley, J. Shi, B. K. Juluri and T. J. Huang, *Lab Chip*, 2009, **9**, 2050–2058.
32 M. Zickar, W. Noell, C. Marxer and N. de Rooij, *Opt. Express*, 2006, **14**, 4237–4249.
33 G. Beadie, J. S. Shirk, A. Rosenberg, P. A. Lane, E. Fleet, A. R. Kamdar, Y. Jin, M. Ponting, T. Kazmierczak, Y. Yang, A. Hiltner and E. Baer, *Opt. Express*, 2008, **16**, 11540–11547.
34 C. Gomez-Reino, M. V. Perez and C. Bao, in *Gradient-Index Optics: Fundamentals and Applications*, ed. C. Gomez-Reino, M. V. Perez and C. Bao, Springer, Heidelberg, 2002, pp. 127–131.
35 B. K. Juluri, S. C. S. Lin, T. R. Walker, L. Jensen and T. J. Huang, *Opt. Express*, 2009, **17**, 2997–3006.
36 Y. N. Xia and G. M. Whitesides, *Annu. Rev. Mater. Sci.*, 1998, **28**, 153–184.
37 http://rsbweb.nih.gov/ij/.
38 J. R. Welty, C. E. Wicks, R. E. Wilson and G. L. Rorrer, in *Fundamentals of Momentum, Heat, and Mass Transfer*, ed. J. R. Welty, C. E. Wicks, R. E. Wilson and G. L. Rorrer, John Wiley & Sons, Inc., 5th edn, 2008, pp. 415–416.
39 S. K. Y. Tang, B. T. Mayers, D. V. Vezenov and G. M. Whitesides, *Appl. Phys. Lett.*, 2006, **88**, 061112.
40 J. T. Blakely, R. Gordon and D. Sinton, *Lab Chip*, 2008, **8**, 1350–1356.
41 C. Liberale, P. Minzioni, F. Bragheri, F. De Angelis, E. Di Fabrizio and I. Cristiani, *Nat. Photonics*, 2007, **1**, 723–727.
42 X. Mao, S. C. S. Lin, C. Dong and T. J. Huang, *Lab Chip*, 2009, **9**, 1583–1589.
43 T. D. Rane, C. M. Puleo, K. J. Liu, Y. Zhang, A. P. Lee and T. H. Wang, *Lab Chip*, 2010, **10**, 161–164.
44 H. Y. Hsu, A. T. Ohta, P. Y. Chiou, A. Jamshidi, S. L. Neale and M. C. Wu, *Lab Chip*, 2010, **10**, 165–172.
45 S. Kühn, E. J. Lunt, B. S. Philips, A. R. Hawkins and H. Schmidt, *Lab Chip*, 2010, **10**, 189–194.
46 S. Kühn, P. Measor, E. J. Lunt, B. S. Phillips, D. W. Deamer, A. R. Hawkins and H. Schmidt, *Lab Chip*, 2009, **9**, 2212–2216.
47 Y. N. Wang, Y. J. Kang, D. Y. Xu, L. Barnett, S. A. Kalams, D. Y. Li and D. Q. Li, *Lab Chip*, 2008, **8**, 309–315.
48 J. Shi, D. Ahmed, X. Mao, S. C. S. Lin and T. J. Huang, *Lab Chip*, 2009, **9**, 2890–2895.
49 J. Shi, H. Huang, Z. Stratton, A. Lawit, Y. Huang and T. J. Huang, *Lab Chip*, 2009, **9**, 3354–3359.
50 J. Shi, X. Mao, D. Ahmed, A. Colletti and T. J. Huang, *Lab Chip*, 2008, **8**, 221–223.